A fast response and recovery H2S gas sensor based on free-standing TiO2 nanotube array films prepared by one-step anodization method

Xin Tong, Wenhao Shen, Xiaoquan Chen, Jean-Pierre Corriou

A fast response and recovery H_2S gas sensor based on free-standing TiO_2 nanotube array films prepared by one-step anodization method

Xin Tong[a], Wenhao Shen[a,*], Xiaoquan Chen[a], Jean-Pierre Corriou[b]

[a] State Key Laboratory of Pulp and Paper Engineering, South China University of Technology Guangzhou, 510640, P.R. China

[b] Laboratoire Réactions et Génie des Procédés, UMR 7274-CNRS, Lorraine University, ENSIC, 1, rue Grandville BP 20451, 54001 NANCY Cedex, FRANCE

*Corresponding author.

Tel.: +86 20 87111634

E-mail address: ppwhshen@scut.edu.cn (Wenhao Shen)

Abstract

Free-standing TiNT array film was successfully synthesized by a one-step anodization method. The characteristic techniques including scanning electron microscopy (SEM), transmission electron microscopy (TEM) and X-ray diffraction (XRD) were adopted to characterize the morphology and chemical composition of the TiNT array film. Subsequently, gas sensor based on the TiNT array film was fabricated and its sensing performance toward H_2S was investigated. The results showed that the optimum operating temperature to detect H_2S gas was 300℃, the detection range to H_2S gas was 1-50 ppm with the response value of 4.5-26.2, and a

good linearity of sensing characteristics could be observed. Meanwhile, the response and recovery time of the sensor to 50 ppm H_2S gas were as low as 22 s and 6 s, respectively. In addition, mechanisms of the development of the free-standing TiNT array film and the sensor towards H_2S were discussed. In conclusion, its outstanding sensing properties and readily fabrication of the TiNT array film sensor presented the potential industrial applications.

Keywords: TiO_2 nanotube array film; Free-standing; Anodization; H_2S; Gas sensor

1. Introduction

Hydrogen sulfide (H_2S) is one of the main pollutants produced in various industrial processes. It is colorless, highly toxic, extremely flammable and corrosive in nature [1,2]. Humans exposed to H_2S at low concentrations suffer eye irritation, olfactory fatigue, and damage to the lungs and nervous system. The inhalation of 320 ppm H_2S may collapse the heartbeat leading to sudden death [3,4]. Thus, from a safety point of view, the monitoring of H_2S is crucial in many industrial areas.

Recently, there have been many reports on the H_2S sensors based on metal oxide semiconductors, such as: Fe_2O_3 [5], CuO [6], ZnO [7], WO_3 [8] etc. In the past decades, due to its interesting physical and chemical properties, titanium dioxide (TiO_2) has been considered to be one of the important multifunctional materials with photocatalytic, photoelectrochemical and gas sensor applications. In particular, being similar to other metal oxide semiconductors, TiO_2 also has shown responses to several

kinds of gases [9-11]. Although the detection results have been reported so far, the research on the H_2S sensors with TiO_2 is relatively new and their gas-sensing performance needs to be improved [12,13]. Thus, developing new sensing material with high response, good selectivity and quick response is extremely important for real-time monitoring of H_2S.

Recently the improved surface reactivity of TiO_2 systems has been reported, where the nanowires, nanorods and nanotubes have been used [14-16]. One of the main features of these nanostructures is the large specific surface area that makes them attractive for use as the sensitive films for gas sensors, which can improve the gas sensitive performance effectively. Although the TiO_2 nanotube (TiNT) arrays have been successfully synthesized with the electrochemical anodization method, most sensitive performance were just obtained on the generated nanotube array without assembling, which hinders the practical application of TiNT [16-18].

Several methods for the preparation of the independent TiO_2 nanotube arrays have been reported, which are classified into physical methods and chemical methods. The physical methods mainly included solvent evaporation film separation [19] and ultrasonic oscillation [20], whose main drawback was that it was difficult to obtain the large complete independent TiO_2 thin film, and the morphology of the titanium tube was prone to be destroyed. The chemical methods mainly included the secondary anodic oxidation [21] and the dissolution method in chemical solution [22]. In other words, the secondary treatments were obligatory during the preparation process of the TiNT array membrane and the thick film restricted their feasibility for gas sensing

applications.

In this work, in Section 3.1, the process of obtaining a complete free-standing TiNT array membrane by the anodic oxidation method followed by annealing without any secondary treatments is presented. In Section 3.2, the morphology of the TiNT membrane obtained with this cost-effective and time-saving method is studied. In Section 3.3, obtained free-standing array film of TiNT to fabricate a gas sensor is explained and its gas sensing performances to H_2S are carefully investigated. In Section 3.4, the gas sensing mechanisms of the developed free-standing TiNT array film are also analyzed in the paper.

2. Materials and methods

2.1 Synthesis of TiO_2 nanotube array

Prior to the anodization experiments, the titanium foils (99.7% purity, 0.01 mm thickness) were ultrasonically cleaned for 10 min in acetone, alcohol and deionized water in sequence, finally dried in air. The anodization was conducted in a two-electrode electrochemical cell with a platinum foil as cathode and the titanium foil as anode at a constant potential. All the anodization experiments were carried out at room temperature with stirring.

The anodizing was carried out at 30 V for 2 h using a direct-current stabilizer (TASI-1305, Suzhou TASI electronic CO., LTD.). The growth of the nanotube arrays was obtained using a glycol solution with 0.55 wt% ammonium fluoride and 20 wt% deionized water. After that, the anodized titanium foil was rinsed with deionized water,

and dried in air. The samples were heated up to 100℃, 200℃, 300℃, 400℃ for 10 min orderly, at the rate of 10℃/min, and then annealed at 450℃ for 2 h in the air.

2.2 Characterization of the nanotube array film

The morphologies of the free-standing TiNT array film samples were characterized by the scanning electron microscopy (SEM) and the energy-dispersive X-ray spectroscopy (EDS) (Merlin, Zeiss, Germany).

The X-ray diffraction (XRD) patterns were recorded at the room temperature with Cu Kα radiation of 0.15418 nm in an X-ray diffractometer (D8 ADVANCE, Bruker, Germany), using a generator voltage of 40 kV and current of 40 mA. The data were collected for scattering angles (2θ) ranging from 10° to 85° with a step of 0.02° for 2 s per point. The transition electron microscope (TEM) was performed with the transmission electron microscopy (JEM-2100F, Japan).

2.3 Sensor fabrication

For fabrication of the gas sensor, the alumina plate (1.0×1.5 mm) with the gold electrodes and heating layer processed by the method of screen painting printing [23, 24] was used as the substrate. In order to remove the stain, the substrates were immersed in acetone, ethanol and deionized water, successively, for 10 min.

A mixture of 10 mL of titanium tetraisopropoxide solution in ethanol with terpilenol in volume ratio of 6: 3: 2 was painted onto the side of the substrate for facilitation the later adhesion for the free-standing TiNT array membrane. Then, the

sensor attached with the nanotube layer was heated at 350℃ for 30 min. After heating treatment, the adhesive was transformed into the TiO_2 interlayer, which let the connection between the substrate and TiNT array film became more compact. Because of the little amount of TiO_2, the contribution of the TiO_2 interlayer to the sensing performance can be considered negligible.

The schematic diagram of the sensor structure is shown in Fig. 1 for the sensing measurements. To improve its stability and repeatability, the gas sensor was welded on the pedestal, followed by aging at 450℃ for 72 h in air.

2.4 Gas sensing measurements

The measurement of the gas sensing performances of the sensor were conducted by a WS-30A Gas Sensing Measurement System (Weisen Electronic Technology Co., Ltd., China). Fig. 2 displays a schematic diagram the whole measuring process. The final concentration of the H_2S inside the test chamber was controlled by mass flow controllers (MFC) connected to calibrated bottles of N_2 and H_2S. The relative humidity (RH) was about 50% in the whole testing process.

As shown in the measuring electric circuit (Fig. 2), in the sensing test process, an appropriate bias voltage (V_t=5 V) is applied. The working temperature of the sensors could be controlled from room temperature to 500℃ by the heating voltage V_h. R_s is a resistor of the sensor and R_l is a load resistor connected in series with the gas sensor.

The gas response was defined as the ratio of the stationary electrical resistance of the sensor in the air R_a to the resistance in the test gas R_g, that is, Response=R_a/R_g.

The response and recovery times of the films were calculated from the response curves automatically. The response and recovery times were defined as the time required for a change of the response value to reach 90% of the equilibrium value and falls to 10% of its maximum sensitivity after injecting and removing the detected gas, respectively.

3. Results and discussions

3.1 Development of the free-standing TiNT array film

The formation of the free-standing TiNT array film by electrochemical anodization is a complex process, its growth mechanism can be represented by Fig. 3. The overall process of oxide formation was divided into four steps [25-27]:

(1) Formation of the TiO_2 via oxidation

At the beginning of this stage, the concentration of Ti^{4+} was raised by the electrochemical etching of the Ti, then the amorphous TiO_2 film was formed through the reaction between Ti^{4+} and adsorbed O^{2-} on the surface of the electrode.

(2) Formation of the pores

After the formation of the initial TiO_2 layer, fluorine ions could attack the oxide leading to the formation of the pores through the produced water-soluble $[TiF_6]^{2-}$ species. With the extension of the oxidation time, the ordered pores were formed on the surface of the TiO_2 layer. Under the effect of electrochemical etching, the depth of the pores would be increased gradually.

(3) Formation of the TiO_2 nanotube array

The electric field intensity on the concave surface of the pores is lower than outside the pores, hence the corrosion rate of titanium dioxide on these sites is the fastest [28]. With the migration of the charge density to the bottom of the nanotubes, the oxidation film was dissolved along the axial direction of the tubes, gradually forming the tubular structure film layer. However, as shown in Fig. 4 (a), as time goes on, the dissolving speed decreases, so that the thickness of the nanotubes wall gradually increased from top (13 nm) to bottom (36 nm).

Moreover, the metallic region between the tube holes also undergoes a similar transition leading to the formation of the array of relatively independent nanotubes (Fig. 4).

(4) Formation of the free-standing TiNT array film

The tube length is governed by competition between anodic oxide formation and its chemical dissolution. While oxygen and fluorine ions around the titanium are gradually consumed, both the fluorine ion etching rate and the TiO_2 forming rate begin to decrease until reaching an equilibrium. As shown in Fig. 5, when the reaction lasts 4 hours, the Ti substrate had been completely oxidated to TiNT array. However, as presented in Fig. 4 (b-c), after 4 h, the pore mouths have been eroded. When the reaction duration is increased to 6 h, the tube holes are more dissolved and begin to collapse.

With the progress of oxidation time, the length of the TiNT increases leading to an increased strain strength between the TiNT array film and Ti substrate. When the reaction time attains 2 hours, the compressive stress reaches the critical debongding

stress. Moreover, annealing modifies the interface between them. Hence, the nanotube array film can be desquamated off naturally after heating treatment [29].

In order to ensure the integrity of nanotube mouth and membrane, the oxidation time was taken as 2 hours in the subsequent experiments.

3.2 Structural and morphological characteristics

Vertically oriented, high aspect ratio TiNT arrays grown by anodic oxidation of Ti foil were flaked off naturally after the annealing treatment. The transparent TiNT peeled off the Ti foil is shown in Fig. 6 (a). Fig. 6 (b-d) present the SEM images with side, top and bottom views of the free-standing TiNT array film. The average inner diameter of the nanotube was around 110 nm with a wall thickness of 13 nm and the tube length was 3.8 μm. The hollow structure and the wall of the TiNT can be seen clearly in Fig. 7. The enlarged TEM image shows a fringe pattern, where the resolved spacing between the two parallel neighboring fringes is 0.35 nm, corresponding to the interplanar distance of the {101} lattice planes in anatase TiO_2 (Fig. 4b) [30,31].

To better understand the crystalline form and the surface element distribution, the XRD and EDS were performed. Fig. 8 shows the X-ray diffraction (XRD) patterns of the TiNT array calcined at 450℃ for 2 h. It can be seen that the phase present was anatase (JCPDF No. 21-1272). The diffraction peaks at 2θ= 25.1°, 37.4°, 47.8°, 53.8°, 54.9° and 62.8° are identified to be the (101), (004), (200), (105), (211) and (204) crystal faces, respectively [12,32]. These crystalline peaks indicate that the crystal structure of TiNT film is the anatase phase. Moreover, Fig. 9 reveals the

stoichiometric TiO_2 composition of the film measured by the energy dispersive spectroscopy method. Hence, the titanium nanotubes are mainly composed with the titanium and oxygen element, which proved that the compound was titania.

3.3 Gas sensing properties

From the results mentioned above, we had obtained the free-standing TiNT array film prepared by one-step electrochemical anodization followed by thermal annealing.

3.3.1 Optimum operating temperature for gas sensing

In order to evaluate the optimum operating temperature, the sensor was exposed to 50 ppm H_2S at temperatures ranging from room temperature to 400℃. The response of the sensor to H_2S with respect to its operating temperature is presented in Fig. 10.

Over this temperature range, the response of the sensor increased with the temperature up to 300℃ and then started to decrease. At temperatures below 300℃, an increase in the operating temperature promoted H_2S chemisorption and the reaction between the adsorbed H_2S molecules and the adsorbed oxygen species, leading to an enhanced response to H_2S gas. When the operating temperature was 300℃, the response value was 26.2. In contrast, at temperatures higher than 300℃, the response to H_2S was reduced due to desorption of H_2S, which decreased the amount of H_2S adsorbed on the sensor surface [5,33]. Therefore, the optimal operating temperature was 300℃ for the TiO_2 sensor.

3.3.2 Response and recovery time

The response and recovery time are two important parameters for a gas sensor in practical application [34]. Fig. 11 is an image of the real-time gas sensing transient to 50 ppm H_2S at 300℃ drawn to show the moments of gas input and gas stop. The response value increased rapidly when the TiNT sensor was exposed to H_2S gas and returned to the initial value when the H_2S gas supply was stopped and air was introduced. The response and recovery times of the sensor are measured from Fig. 11 and presented in Fig. 12.

From Fig. 12, it can be seen that the sensing films have short response-recovery times, suggesting that the sensors respond quickly to both the injection and removal of the H_2S gas in air. Moreover, the response and recovery times do not dependent on the concentration of H_2S at 1-50 ppm. However, the response times of the sensor exposed to H_2S at 10-50 ppm are longer than at 1-10 ppm. The phenomenon reveals that the response time increases with the increasing concentration of H_2S. When exposed to 50 ppm H_2S at 300℃, the response time and recovery time of the sensor were 22 s and 6 s, respectively.

3.3.3 Effects of gas concentration

The sensitive performance of the sensor was further investigated by exposing the sensors to different concentrations of H_2S gas at the operating temperature of 300℃. The curves of gas response versus time for 1-10 ppm of H_2S gas sensed by the TiNT array film at 300℃ are shown in Fig. 13 (a), where the response amplitude of the

sensor increases with H_2S concentration. Fig. 13 (b) shows that the sensitivity for the TiO_2 sensor is improved with increasing H_2S concentration in the range of 1-50 ppm. The sensor responses toward 1 and 10 ppm are found about 4.5 to 12.4, respectively. It could be clearly seen that the response increases linearly with the concentrations in this range, indicating a good linearity of sensing characteristics. Moreover, when the concentration of H_2S exceeds about 10 ppm, the sensitivity still increases but at a lower rate.

3.3.4 Selectivity studies

The gas sensing selectivity of the TiNT array film was further tested at 300℃ by exposing the sensors to 50 ppm potentially interfering gases including methanol, formaldehyde, benzene, toluene, xylene and n-dodecane vapors, and the results are depicted in Fig. 14. Clearly, the sensor based on the TiNT is the most sensitive to H_2S, whereas it presents a low response to the other interfering gases at the same temperature, implying that the sensor exhibits a better selectivity to H_2S than to other gases.

3.3.5 Stability and repeatability

Thermal stability and repeatability of the sensor had been investigated by repeating experiments for 50 ppm H_2S at 300℃. Fig. 15 displays the measured values for the sensor response versus the storing time. As displayed in the figure, the response results of the sensor possess a variation of ±1.4% from the initial result (26.2)

265 in one month. The free-standing TiNT array film demonstrated a good stability and
266 reproducibility with regard to 50 ppm H_2S gas at 300℃, which indicated a stable
267 morphology and good crystallinity of the fabricated sensing layer.
268
269 **3.4 Gas sensing mechanism**
270 It is well known that the sensing mechanism of TiO_2-based gas sensors belongs
271 to the surface-controlled type, which is based on the change in conductance of the
272 semiconductor [35,36]. When the sensor is exposed to air, electrons in the surface
273 region of the TiO_2 nanotube walls are consumed by the oxygen molecules that are
274 adsorbed on the TiO_2 surface. Then a depletion region is created on the wall of the
275 TiNT, leading to an increase in the electric resistance of the TiNT array film [37].
276 Another point to be noted is that the type of adsorbed oxygen species depends on the
277 working temperature of sensor. The changing process of oxygen molecules on the
278 nanotube surface is illustrated in Eqs. (1-4) [38,39]:
279 $$O_2(\mathrm{g}) \rightarrow O_2(\mathrm{ads}) \quad (1)$$
280 $$O_2(\mathrm{ads}) + \mathrm{e}^- \rightarrow O_2^-(\mathrm{ads}) \quad (\mathrm{T} < 147℃) \quad (2)$$
281 $$O_2^-(\mathrm{ads}) + \mathrm{e}^- \rightarrow 2O^-(\mathrm{ads}) \quad (147℃ < \mathrm{T} < 397℃) \quad (3)$$
282 $$O^-(\mathrm{ads}) + \mathrm{e}^- \rightarrow O^{2-}(\mathrm{ads}) \quad (\mathrm{T} > 397℃) \quad (4)$$
283 When the sensor was exposed to H_2S gas, which was a reducing gas, these
284 chemisorbed oxygen species played a crucial role in enhancing the H_2S gas sensitivity
285 as explained by the schematic diagram in Fig. 16. The H_2S reacted with these oxygen
286 species and got dissociated after releasing trapped electrons to the TiNT via the

speculated reactions given in Eqs. (5-6) [4,12]:

$$H_2S(\mathrm{g}) \rightarrow H_2S(\mathrm{ads}) \quad (5)$$

$$2H_2S(\mathrm{g}) + 6O^-(\mathrm{ads}) \rightarrow 2H_2O(\mathrm{g}) + 2SO_2(\mathrm{g}) + 6\mathrm{e}^- \quad (6)$$

This leaded to an increase in the carrier concentration on the TiO_2 nanotube walls and a decrease in the surface depletion layer width. Hence, there is an increase in the response value as shown in Fig. 11.

Table 1 summarizes the results of gas response to H_2S using various forms of TiO_2. The response and recovery time with most of the H_2S sensors prepared by TiO_2 materials were long, or a modification method was necessary to improve its gas sensitive performances. However, in this work, the response value, response and recovery times of the purified TiNT array film sensor toward H_2S gas were comparable to those of the most other TiO_2 nanomaterials.

The following physical and chemical effects might contribute partly to the enhanced H_2S sensing properties of the TiNT array film sensor: (1) electrons are conducted through the wall of TiNT because of its particular structure, which reduces the recombination of electrons and holes; (2) the TiNT that presents a large surface area due to their tube array structure results in a better sensitivity.

4. Conclusion and perspectives

The free-standing TiNT array film was successfully synthesized by a one-step anodization method. Then the film was fabricated and tested for H_2S gas sensing at low concentrations.

The H_2S sensing properties including operating temperature, reversibility, relationship between sensitivity and H_2S concentration, selectivity and stability were studied. The results showed that the optimum operating temperature to detect H_2S gas was 300℃, the detection range to H_2S gas was 1-50 ppm with the response value of 4.5-26.2, and a good linearity of sensing characteristics could be observed. It is generally accepted that metal oxide gas sensors possess relatively longer response and recovery times. However, the response and recovery time of the sensor to 50 ppm H_2S gas were as low as 22 s and 6 s, respectively. Moreover, the growth mechanism and gas sensing mechanism of the TiNT array film were studied.

It can be seen that the response values, response and recovery times of the sensor were outstanding throughout the tests, which demonstrated that the fabricated TiNT array film sensor presented the potential industrial applications. Moreover, this electrochemical anodization method based on the Ti foil is relatively simple and, hence, induces lower costs and makes it be attractive for developing gas sensors devices.

Acknowledgments

The research was supported by the Research Funds of National Science Foundation of Guangdong, China (No. 2016A030313478), Science and Technology Planning Project of Guangdong, China (No. 2015A020215012), State Key Laboratory of Pulp and Paper Engineering, South China University of Technology (No. 2015C05),

and Science and Technology Program of Guangzhou, China (No. 201607010050).

References

[1] M. Kaur, B.K. Dadhich, R. Singh, KailasaGanapathi, T. Bagwaiya, S. Bhattacharya, et al., RF sputtered SnO_2: NiO thin films as sub-ppm H_2S sensor operable at room temperature, Sens. Actuators B 242 (2017) 389-403.

[2] G.-J. Sun, H. Kheel, J.K. Lee, S. Choi, S. Lee, C. Lee, H_2S gas sensing properties of Fe_2O_3 nanoparticle-decorated NiO nanoplate sensors, Surf. Coat. Technol. 307 (2016) 1088-1095.

[3] M.A. Haija, A.F.S. Abu-Hani, N. Hamdan, S. Stephen, A.I. Ayesh, Characterization of H_2S gas sensor based on $CuFe_2O_4$ nanoparticles, J. Alloys Compd. 690 (2017) 461-468.

[4] T.C. Jagadale, V. Prasad, N.S. Ramgir, C. Prajapat, U.V. Patil, A. Debnath, et al., Greatly enhanced H_2S sensitivity using defect-rich titanium oxide films, RSC Adv. 5 (2015) 93081-93088.

[5] H. Kheel, G.-J. Sun, J.K. Lee, S. Lee, R.P. Dwivedi, C. Lee, Enhanced H_2S sensing performance of TiO_2-decorated α-Fe_2O_3 nanorod sensors, Ceram. Int. 42 (2016) 18597-18604.

[6] Z. Li, N. Wang, Z. Lin, J. Wang, W. Liu, K. Sun, et al., Room-Temperature High-Performance H_2S Sensor Based on Porous CuO Nanosheets Prepared by Hydrothermal Method, ACS Appl. Mat. Interfaces 8 (2016) 20962-20968.

[7] Z.S. Hosseini, A. Mortezaali, A. Iraji zad, S. Fardindoost, Sensitive and selective room temperature H_2S gas sensor based on Au sensitized vertical ZnO nanorods with flower-like structures, J. Alloys Compd. 628 (2015) 222-229.

[8] I. Lee, S.-J. Choi, K.-M. Park, S.S. Lee, S. Choi, I.-D. Kim, et al., The stability, sensitivity and response transients of ZnO, SnO_2 and WO_3 sensors under acetone, toluene and H_2S environments, Sens. Actuators B 197 (2014) 300-307.

[9] Y. Gönüllü, A.A. Haidry, B. Saruhan, Nanotubular Cr-doped TiO_2 for use as high-temperature NO_2 gas sensor, Sens. Actuators B 217 (2015) 78-87.

[10] G. Wu, J. Zhang, X. Wang, J. Liao, H. Xia, S.A. Akbar, et al., Hierarchical structured TiO_2 nano-tubes for formaldehyde sensing, Ceram. Int. 38 (2012) 6341-6347.

[11] E. Sennik, N. Kilinc, Z.Z. Ozturk, Electrical and VOC sensing properties of anatase and rutile TiO_2 nanotubes, J. Alloys Compd. 616 (2014) 89-96.

[12] S. Ma, J. Jia, Y. Tian, L. Cao, S. Shi, X. Li, et al., Improved H_2S sensing properties of Ag/TiO_2 nanofibers, Ceram. Int. 42 (2016) 2041-2044.

[13] P. Chaudhari, S. Mishra, Effect of CuO as a dopant in TiO_2 on ammonia and hydrogen sulphide sensing at room temperature, Measurement 90 (2016) 468-474.

[14] Z. Qu, Y. Fu, B. Yu, P. Deng, L. Xing, X. Xue, High and fast H_2S response of NiO/ZnO nanowire nanogenerator as a self-powered gas sensor, Sens. Actuators B 222 (2016) 78-86.

[15] L.T. Lanh, T.T. Hoa, N.D. Cuong, D.Q. Khieu, D.T. Quang, N. Van Duy, et al., Shape and size controlled synthesis of Au nanorods: H_2S gas-sensing characterizations and antibacterial application, J. Alloys Compd. 635 (2015) 265-271.

[16] P.M. Perillo, D.F. Rodríguez, A room temperature chloroform sensor using TiO_2 nanotubes, Sens. Actuators B 193 (2014) 263-266.

[17] N. Kılınç, E. Şennik, M. Işık, A.Ş. Ahsen, O. Öztürk, Z.Z. Öztürk, Fabrication and gas sensing properties of C-doped and un-doped TiO_2 nanotubes, Ceram. Int. 40 (2014) 109-115.

[18] Y. Gönüllü, A.A. Haidry, B. Saruhan, Nanotubular Cr-doped TiO_2 for use as high-temperature NO_2 gas sensor, Sens. Actuators B 217 (2015) 78-87.

[19] J. Wang, Z.Q. Lin, Freestanding TiO_2 nanotube arrays with ultrahigh aspect ratio via electrochemical anodization, Chem. Mater. 20 (2008) 1257-1261.

[20] M. Paulose, H.E. Prakasam, O.K. Varghese, L. Peng, K.C. Popat, G.K. Mor, et al., TiO_2 nanotube arrays of 1000 mu m length by anodization of titanium foil: Phenol red diffusion, J. Phys. Chem. C 111 (2007) 14992-14997.

[21] W. Yuanhao, L. Lin, Y. Hongxing, The Fabrication of Barrier Layer Free TiO_2 Nanotube Arrays and its Application for Highly Efficient Dye-sensitized Solar Cells, Energy Procedia 61(2014) 2608-2612.

[22] S.P. Albu, A. Ghicov, J.M. Macak, R. Hahn, P. Schmuki, Self-organized, free-standing TiO_2 nanotube membrane for flow-through photocatalytic applications, Nano Lett. 7 (2007) 1286-1289.

[23] D.S. Hwang, C.H. Park, S.C. Yi, Y.M. Lee, Optimal catalyst layer structure of polymer electrolyte membrane fuel cell, Int. J. Hydrogen Energy 36 (2011) 9876-9885.

[24] W. Zhang, H. Zhang, S.E. Williams, A. Zhou, Microfabricated three-electrode on-chip PDMS device with a vibration motor for stripping voltammetric detection of heavy metal ions, Talanta 132 (2015) 321-326.

[25] V.C. Anitha, A.N. Banerjee, S.W. Joo, B.K. Min, Barrier-oxide layer engineering of TiO_2 nanotube arrays to get single- and multi-stage Y-branched nanotubes: Effect of voltage ramping and electrolyte conductivity, Mater. Sci. Eng. B 195 (2015) 1-11.

[26] H. Li, N. Tang, H. Yang, X. Leng, J. Zou, Interface feature characterization and Schottky

397 interfacial layer confirmation of TiO_2 nanotube array film, Appl. Surf. Sci. 355 (2015) 849-860.
398 [27] Y. Li, Q. Ma, J. Han, L. Ji, J. Wang, J. Chen, et al., Controllable preparation, growth
399 mechanism and the properties research of TiO_2 nanotube arrays, Appl. Surf. Sci. 297 (2014)
400 103-108.
401 [28] J. Tao, J. Zhao, C. Tang, Y. Kang, Y. Li, Mechanism study of self-organized TiO_2 nanotube
402 arrays by anodization. New J. Chem. 32 (2008) 2164-2168.
403 [29] J.-p. Zou, R.-z. Wang, Debonding phenomenon of TiO_2 nanotube film, Trans. Nonferrous Met.
404 Soc. China 22 (2012) 2691-2699.
405 [30] Y. Kwon, H. Kim, S. Lee, I.-J. Chin, T.-Y. Seong, W.I. Lee, et al., Enhanced ethanol sensing
406 properties of TiO_2 nanotube sensors, Sens. Actuators B 173 (2012) 441-446.
407 [31] Y. Chen, W.Z. Li, J.Y. Wang, Y.L. Gan, L. Liu, M.T. Ju, Microwave-assisted ionic liquid
408 synthesis of Ti^{3+} self-doped TiO_2 hollow nanocrystals with enhanced visible-light photoactivity,
409 Appl. Catal. B 191 (2016) 94-105.
410 [32] P.M. Perillo, D.F. Rodríguez, Low temperature trimethylamine flexible gas sensor based on
411 TiO_2 membrane nanotubes, J. Alloys Compd. 657 (2016) 765-769.
412 [33] H. Zhang, J. Feng, T. Fei, S. Liu, T. Zhang, SnO_2 nanoparticles-reduced graphene oxide
413 nanocomposites for NO_2 sensing at low operating temperature, Sens. Actuators B 190 (2014)
414 472-478.
415 [34] Z. Li, Y. Huang, S. Zhang, W. Chen, Z. Kuang, D. Ao, et al., A fast response & recovery H_2S
416 gas sensor based on alpha-Fe_2O_3 nanoparticles with ppb level detection limit, J. Hazard. Mater.
417 300 (2015) 167-174.
418 [35] Z.P. Tshabalala, D.E. Motaung, G.H. Mhlongo, O.M. Ntwaeaborwa, Facile synthesis of

improved room temperature gas sensing properties of TiO_2 nanostructures: Effect of acid treatment, Sens. Actuators B 224 (2016) 841-856.

[36] L. Liu, X. Li, P.K. Dutta, J. Wang, Room temperature impedance spectroscopy-based sensing of formaldehyde with porous TiO_2 under UV illumination, Sens. Actuators B 185 (2013) 1-9.

[37] S. Lin, D. Li, J. Wu, X. Li, S.A. Akbar, A selective room temperature formaldehyde gas sensor using TiO_2 nanotube arrays, Sens. Actuators B 156 (2011) 505-509.

[38] C. Xiang, Z. She, Y. Zou, J. Cheng, H. Chu, S. Qiu, et al., A room-temperature hydrogen sensor based on Pd nanoparticles doped TiO_2 nanotubes, Ceram. Int. 40 (2014) 16343-16348.

[39] M.E. Franke, T.J. Koplin, U. Simon, Metal and metal oxide nanoparticles in chemiresistors: does the nanoscale matter?, Small 2 (2006) 36-50.

441 **Table 1.** Comparison of the sensor responses to H_2S with different forms of TiO_2.

No.	Morphology	Crystal Structure	Response ($R=R_a/R_g$)	Concentration (ppm)	Temperature (℃)	Response time (s)	Recovery time (s)	Reference
1	Ag-doped TiO_2 nanofiber	Anatase & rutile	8.5	100	350	-	-	Ma et al., 2016
2	TiO_2 nanoparticle-decorated Fe_2O_3 nanorods	anatase	7.4	200	300	150	157	Kheel et al., 2016
3	TiO_2-Al_2O_3	rutile	38.7	1000	650	390	480	Arafat et al., 2017
4	CuO doped TiO_2 nanoparticle	anatase	1.77	50	Room temperature	14	22	Chaudhari and Mishra, 2016
5	TiO_2 nanoplates	anatase	4.8	10	300	10	-	Guo et al., 2016
6	TiO_2 nanowires	rutile	11	80	140	-	-	Munz et al., 2013
7	TiO_2 pellet	rutile	275	10	100	150	2500	Jagadale et al., 2015
8	**Free-standing TiNT array film**	**anatase**	**26**	**50**	**300**	**22**	**6**	**Our work**

442

Figure(s)

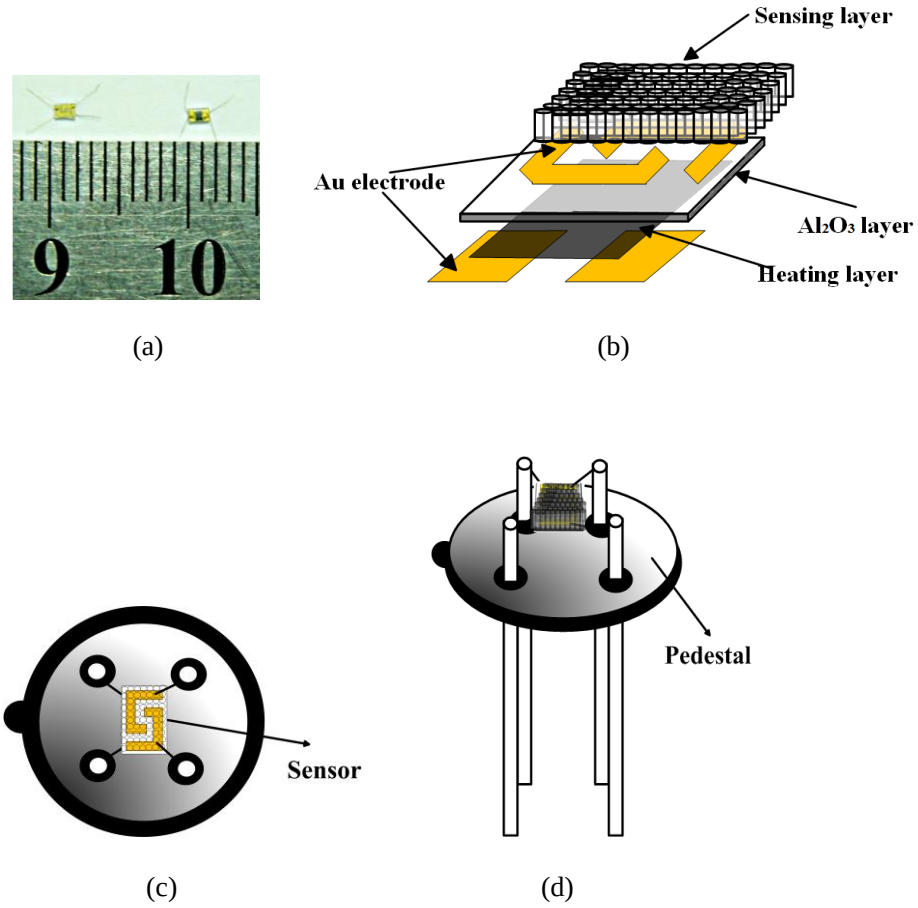

Figure 1. (a) Photographs of the blank sensor. (b)A schematic illustration of the sensor coated with the sensing material. (c) Top view and (d) side view of the fabricated sensor.

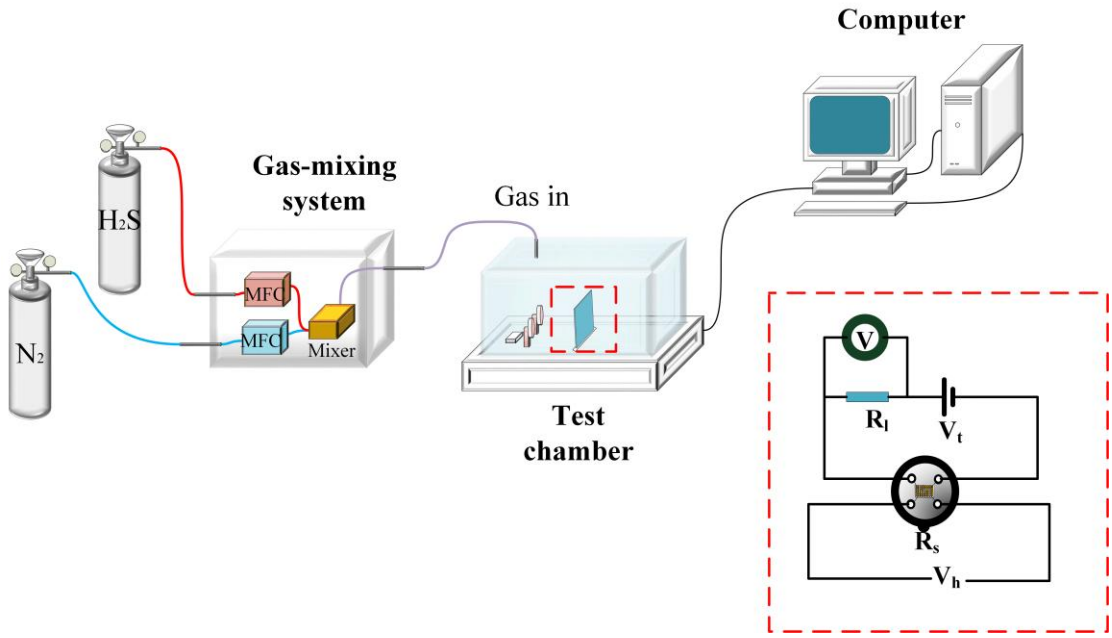

Figure 2. Experimental setup and measuring electric circuit for gas sensing performance.

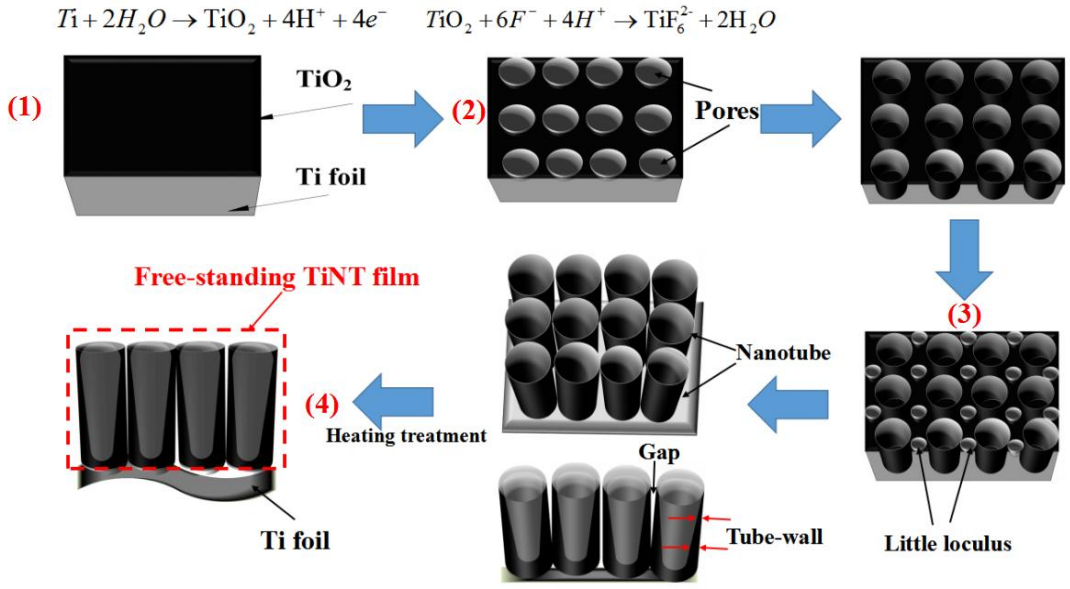

Figure 3. Schematic diagram of the growth mechanism of free-standing TiNT array film.

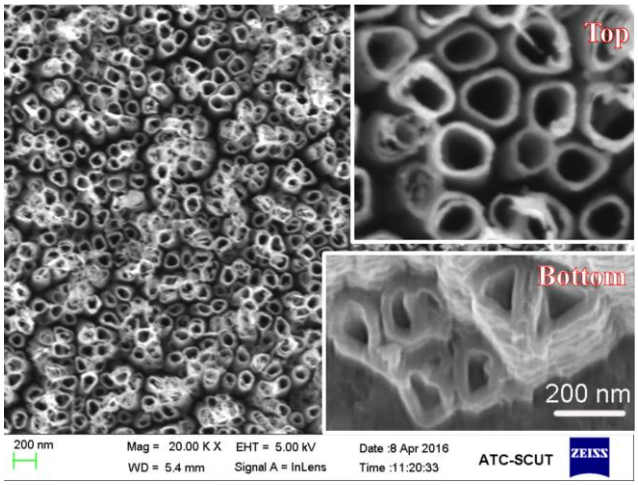

(a) 2h

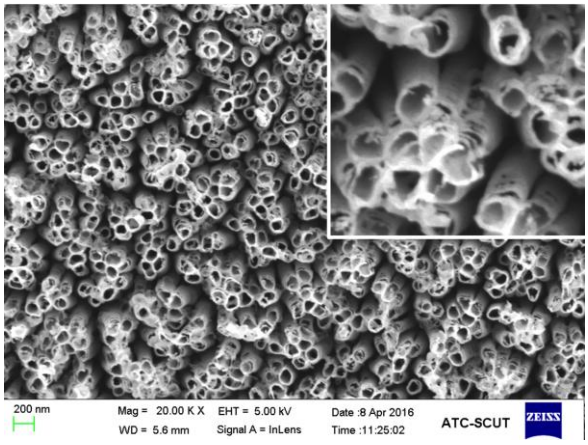

(b) 4h

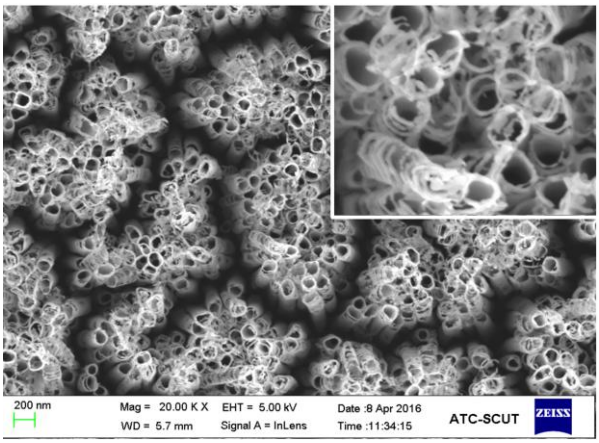

(c) 6h

Figure 4. Top-view SEM images of TiNT array film at different oxidation time.

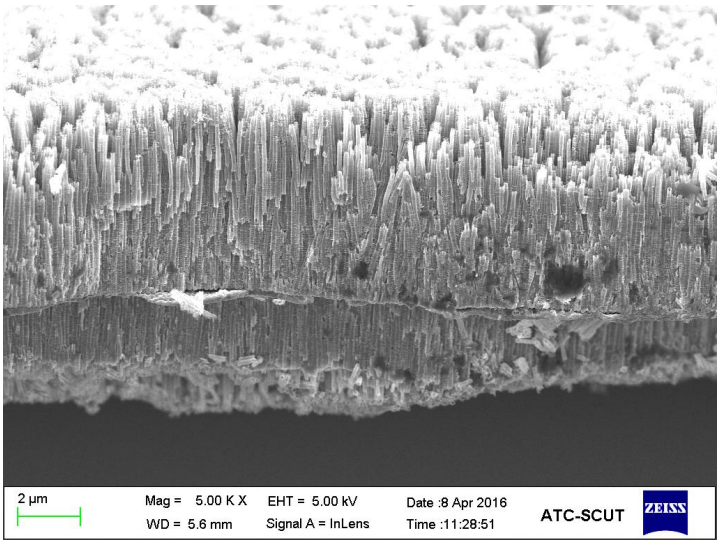

Figure 5. Side-view SEM image of the TiNT array at oxidation time of 4h.

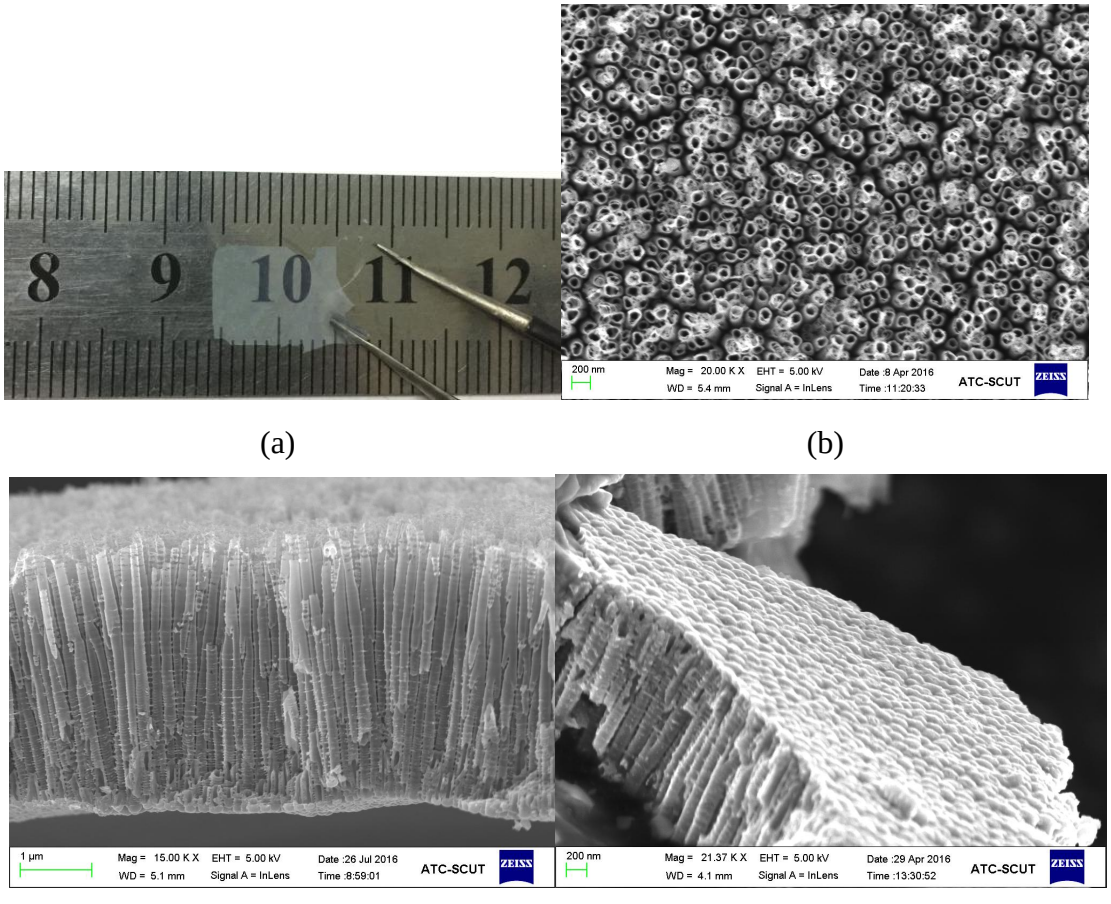

(a) (b)

(c) (d)

Figure 6. (a) Photographic image of the detached TiNT-array film, (b) Top-view SEM, (c) Side-view SEM, (d) Bottom-view SEM image of the TiNT array with the oxidation time of 2h..

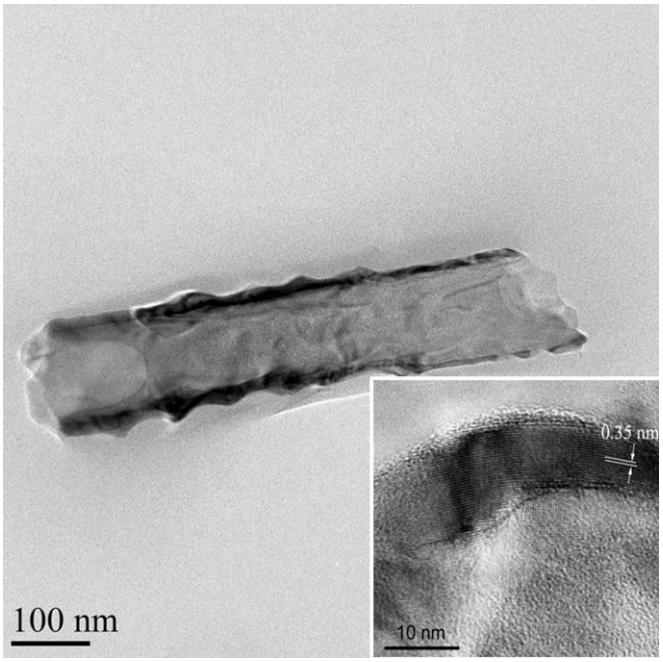

Figure 7. Wide-field TEM and HRTEM images of a single TiNT.

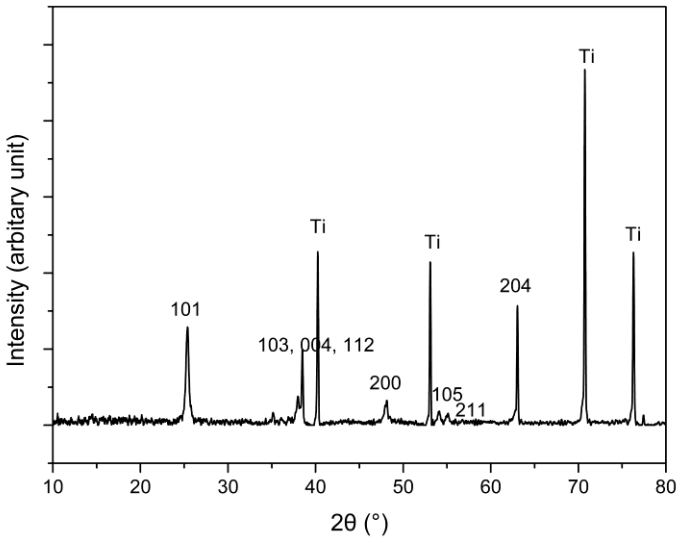

Figure 8. XRD peaks of the TiNT.

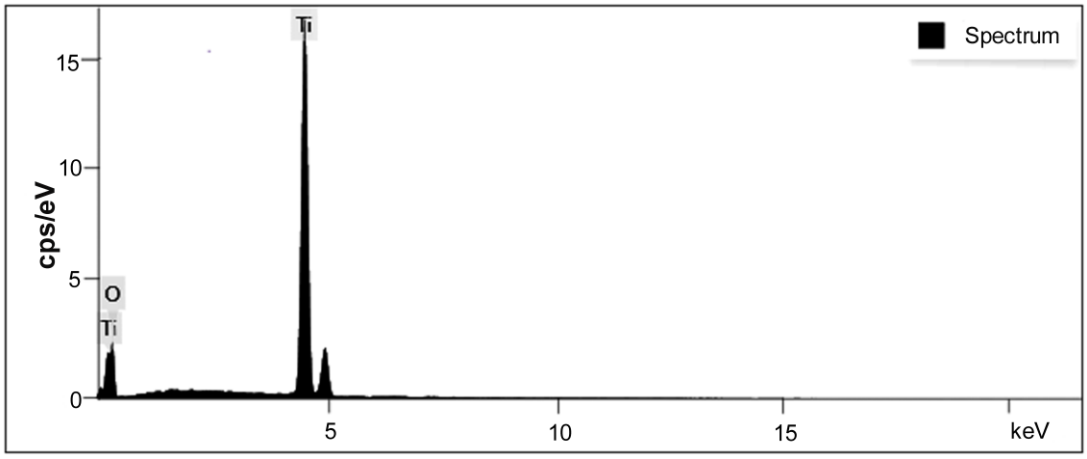

Figure 9. Energy dispersive spectroscopy spectrum of the TiNT arrays.

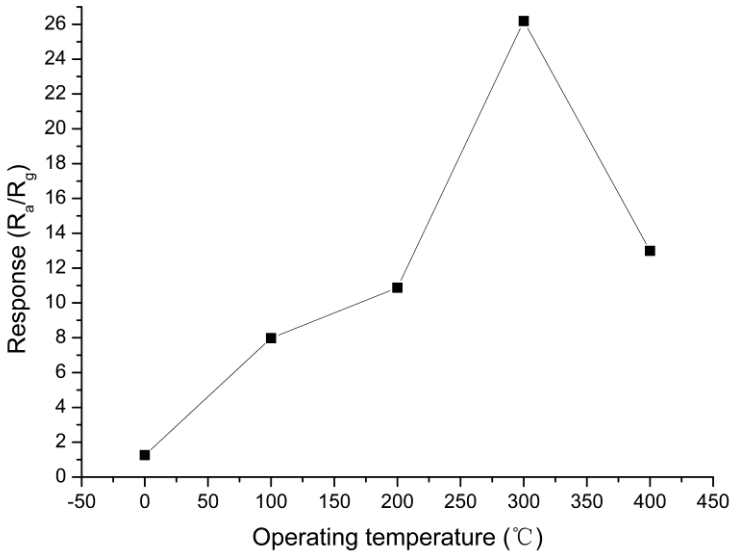

Figure 10. Response values of the free-standing TiNT array film to 50 ppm H_2S at various operating temperatures.

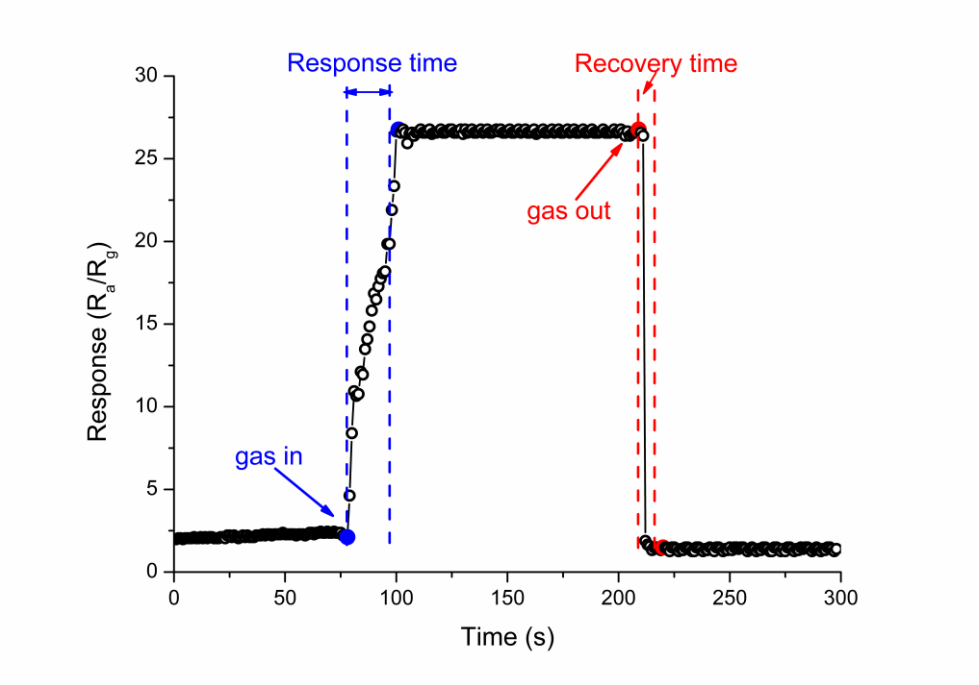

Figure 11. The real-time response curve to 50 ppm H_2S of the sensor at 300℃.

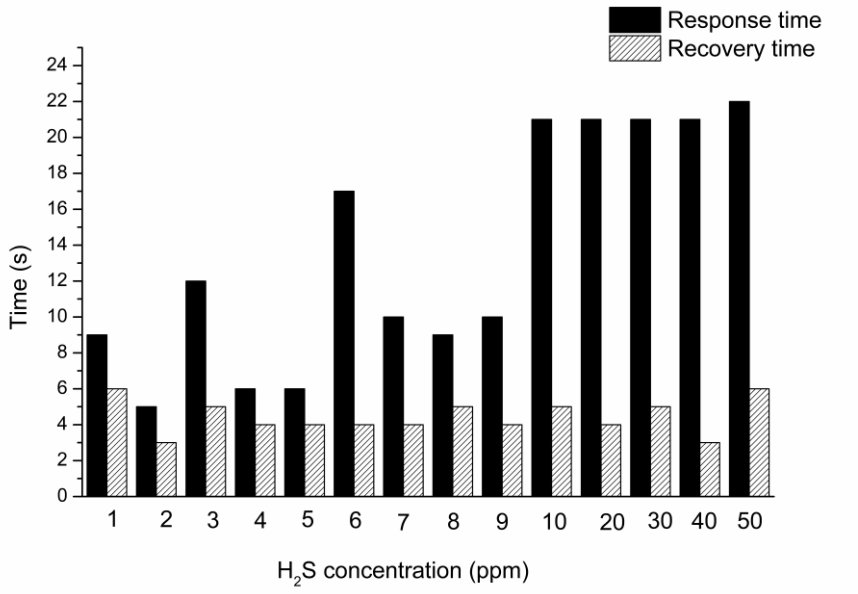

Figure 12. Summary of response time and recovery time of the sensor exposed to H_2S at different concentrations at 300℃.

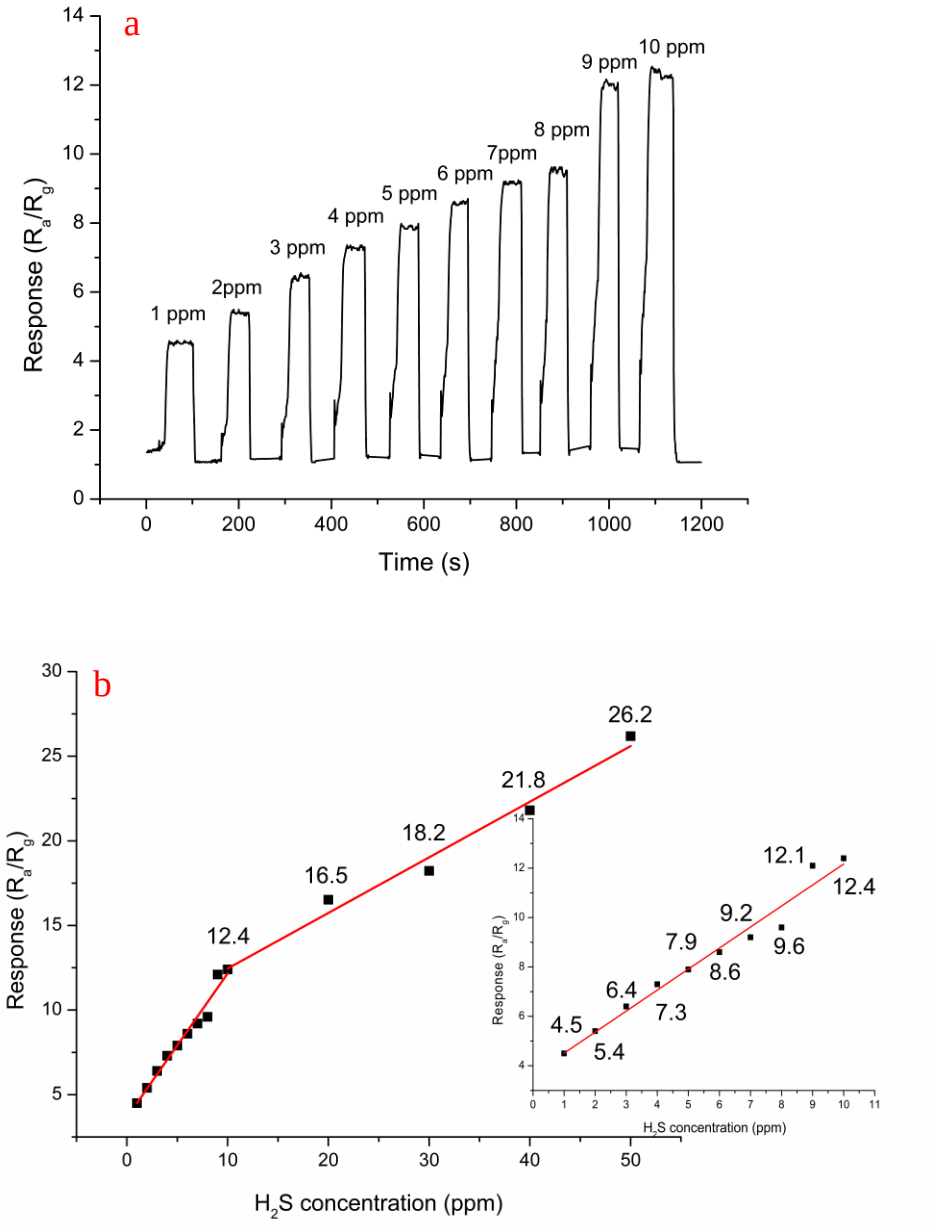

Figure 13. (a) Real-time response curve of the TiNT array film sensor to H_2S with increased concentration at a working temperature of 300℃; (b) Relationship between the sensitivity and H_2S concentration.

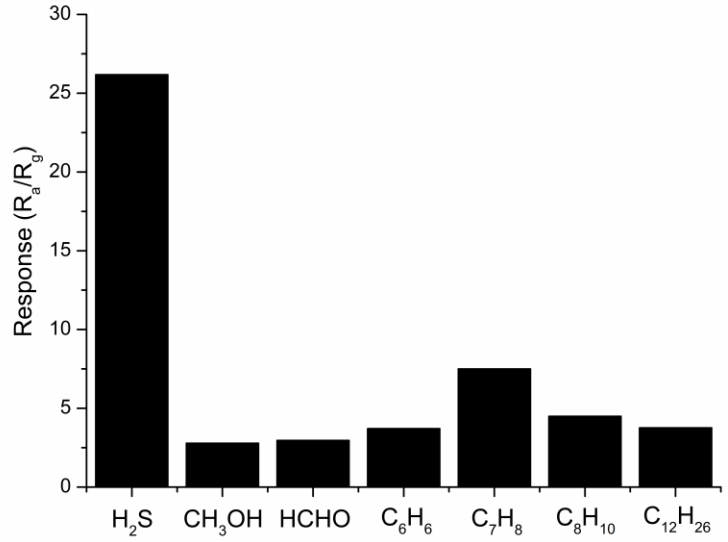

Figure 14. Comparison of sensor response obtained for different gases of 50 ppm.

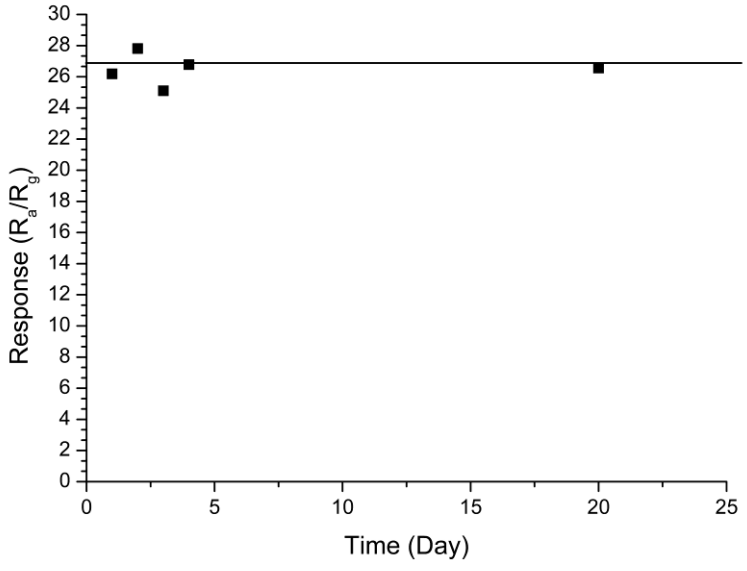

Figure 15. Variation of the sensor response to 50 ppm H_2S at 300 ℃ for different duration times.

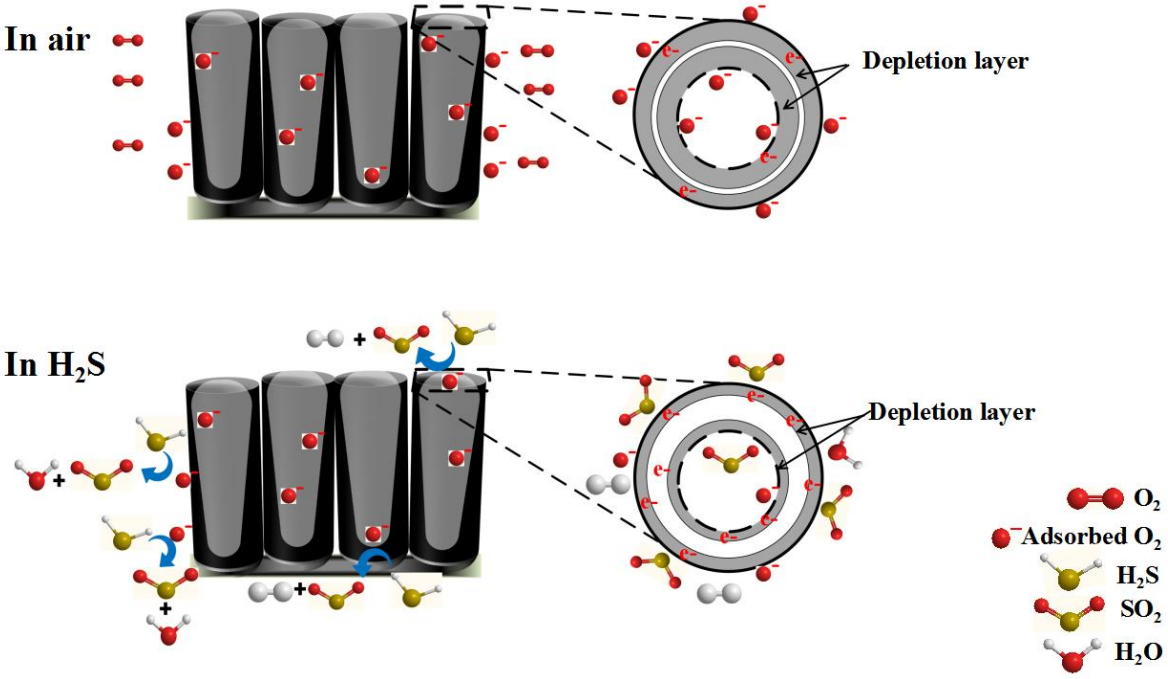

Figure 16. Band diagrams and schematic images of the surface reactions under different atmospheres: (a) exposed in the air (b) in the presence of H_2S gas.